Errors in Bathymetric Retrievals using Linear Dispersion
In 3D FFT Analysis of Marine Radar Ocean Wave Imagery

D. B. Trizna
Naval Research Laboratory, Code 7255
4555 Overlook Avenue
Washington, DC 20375
e-mail: triznad@erols.com
(now at Imaging Science Research, Inc.)

ABSTRACT

The phenomenon of ocean wave-shoaling, and the associated reduction of ocean wave phase speed with decreased water depth, provides useful information for inferring water depth D (bathymetry) in coastal environments. One strategy for relating D to phase speed C and wave-vector K, of long wave length ocean waves, involves using the one-dimensional, linear (gravity wave) dispersion relationship $C^2=g*\tanh(KD)/K$. In principle, this approach has limitations because the approach is based on a WKB approximation, so it cannot be applied when D varies appreciably over the wavelength of a shoaling-wave. Also, the approach is restricted to waves that have small wave-height. In the present paper, we use a set of marine radar image sequences and apply this linear approximation, using a 3-D FFT analysis of 88 sets of image sequences spaced half an hour apart. We invert the dispersion relation to solve for D. Depths between 3.6 and 5.8 meters were tested, for RMS wave heights offshore between .8 and 3 meters. We show that for low to moderate wave heights, the approach does generally retrieve the correct depth in water depths of five meters and greater for moderate wave RMS heights. However, an increase in the RMS wave-height from 1 m to 3.5 m produced a much poorer depth estimate, proving the need for an application of a non-linear wave model to the problem. The errors also increase with shallower depths, as expected as the error dependence on depth and wave height is determined.

INTRODUCTION

The utilization of ocean wave-shoaling photographic imagery, and the observed reduction of ocean wave phase speed with decreased water depth, was used as early as WW-II to provide useful estimates of bathymetry in coastal environments. The method depended upon using a ruler to estimate the direction of wave crest travel, and the horizontal displacement of the crests, to determine a phase velocity for the wave train. With knowledge of deep-water wavelengths from associated line-scan image sequence imagery, one could estimate the expected phase velocity in deep water, C, and estimate the depth using the shallow water dispersion relation.

Some of the first quantitative work using time sequential imagery to determine the change in the frequency-wave number dispersion relation was conducted using marine radar imagery to measure surface

currents (Young, et al, 1985). The linear dispersion relation in shallow water can be expressed by the Ω-K relationship in shallow water of depth, D, with surface current vector, **V**:

$$\Omega^2 = gK \tanh(KD) + \mathbf{V}.\mathbf{K} \quad (1)$$

The departure from the deep water dispersion curve, in which the hyperbolic tangent term is one and **V** is zero, can be established using three dimensional FFT processing of time-sequential imagery of the ocean surface of any type to estimate the depth and current, but not independently of one another. This marine radar work continues (Senet, et al, 1997), and it has also been applied to infrared imagery of near shore shoaling waves (Dugan, et al, 1996, 1997), and more recently to video time sequential imagery (Stockdon & Holman, 2000). In none of these works, however, has the issue of the breakdown of the linear dispersion relation for steep non-linear waves been addressed. Grilli (1998) addressed this issue using non-linear models, but without data against which to compare. As this approach of monitoring coastal bathymetry and surface currents appears to be amenable to inexpensive and continuous radar or video monitoring, it appears that the effects of wave steepness and the onset of non-linear effects needs to be addressed more quantitatively than it has been to date. It is the object of this work to begin such a study.

In this work we test this model using three dimensional Fourier Transform processing of sets of 32 image sequences, taken 1.85 s apart, of marine radar images of shoaling waves at the US Army Coastal Engineering Research Center (USACE), Field Research Facility (FRF) experimental pier at Duck, NC. We demonstrate that the method begins to fail for increasingly high wave conditions, by comparing the measured position of the energy peak in the Ω-K cube with the expected position for the reported depths for four different locations offshore with increasing depth. We apply the analysis to a data set collected over a 36-hr time period during the passage of Hurricane Fran offshore of the USACE Field Research Facility at Duck, NC site.

EXPERIMENT DESCRIPTION

Data were collected during the Duck'96 experiment at the USACE FRF, every 30 minutes continuously. At each collection 32 rotations of the antenna were recorded, 1.85-s apart. Figure 1 shows an example of a single radar image, with the shore normal direction facing downward. The range covered is 2400 m in radius, and the image of the pier is evident as a bright line perpendicular to shore. The brightest spot on the pier is a trailer near the end, and a second-time-around echo can be seen at twice the distance due to a reflection from the shore laboratory back out to the trailer and back again. A description of the stages of recording and analysis for such data has been given previously (Trizna & Carlson, 1996). Data were sampled in radial coordinates, then transformed to Cartesian to produce such images. For light to moderate conditions, a 6-m range spatial resolution is typically used, but for virtually all of the data considered here 12-m resolution was used, allowing longer ranges to be samples for the same data storage requirements. The stronger radar scatter occurred due to

the stronger winds and strong radar echoes from the passage of Hurricane Fran offshore during the period considered. This allowed waves to be imaged farther off shore than normally observed with the radar, due to the offshore extended region of wave breaking that occurred due to shoaling of these steep waves.

The marine radar is horizontally polarized, to minimize sea 'clutter' for radar target tracking applications compared to vertical polarization (See, for example, Trizna, 1991a, 1991b). Thus, small-scale breaking waves are typically responsible for the image brightness at the low grazing angles encountered here (1 to 10^{o}), typically near the long wave crests. (See, for example, Trizna & Carlson, 1996 Trizna, 1997). Such a process forms effectively a filter on shorter gravity waves in the radar image spectrum, so that a modulation transformation function is not applicable for purposes of relating intensity to wave height directly. The radar response is highly non-linear for horizontal polarization, and virtually only the wave crests are tracked using this geometry. However, the Fourier analysis does allow the phase velocity of these waves to be estimated accurately, through 3-D Fourier Transform analysis of a sequence of images as we show now.

Small windows of 40 by 40 points were extracted centered at five different depths, measured during the Duck '96 experiment: 3.7, 4.5, 5.0, 5.4 and 5.8 m. Wavenumber FFT's of 64 x 64 points were calculated, using zero padding beyond the 40 data pints. Analysis was done using 32 x 32 point windows also, using 32-point FFT's, but these resulted in noisier retrieved-depth values. There is a slight depth variation across the 40 point window, which can account for a spectra spread in the wavenumber domain, due to the wave becoming shorter as it shoals into shallower water. We assume that the center wavenumber value of the spectral peaks corresponds to the depth at the center of the data window. Slightly deeper and shallower water either side of center normal to shore would be expected to cause a spread of the spectrum either side of the center value in the K_x-K_y planes.

RESULTS

Figure 2 shows 8 frequency planes of 16 of the analysis (#'s 3 through 10) for a 3-D FFT during the period of low wave conditions early in the sequence, with the frequency of each image labeled accordingly. Note that the propagation direction ambiguity is resolved compared to single image wavenumber FFT analysis. For 32 image sequences spaced 1.85 s apart, 16 positive frequency K_x-K_y spectra result, as well as a symmetric set of 16 negative frequency spectra, so that only one or the other set need be considered. Radar image intensity wave number spectra are shown, and both the longest (Spectrum #1 - 19-s) and intermediate waves (Spectrum #8 - 6-s) are well represented in spectral energy by the integration that occurs over 32 time steps. The images are labeled in $2\pi/K$, with corresponding ocean wavelengths at values of 24, 32, 48, and 96 m. Figure 3 shows a similar set of plots for a period of highest wave activity on Julian day 250. The peak of the spectrum now is seen

to lie far from the expected shallow water value on the red circle, so that the this depth difference is interpreted as the error due to non-linear wave effects for the higher wave conditions.

For 32 images 1.85-s apart, a frequency resolution of 0.01689 Hz is achieved. The 3rd, 4th , and 5th in Figure 3 images show energy near the inner most 64-m circle, with energy overlap through the two spectra either side of the strongest spectrum at 0.068 Hz; i.e., spectral energy occurs in each of the adjacent spectra at the peak wavenumber of the center one, but with weaker amplitude. The inner white circle is the expected position of the spectral energy if the waves travel according to the deep water phase velocity, while the red circle is the location expected for the measured depth. For this case of light winds and waves, the linear dispersion relation is satisfied satisfactorily in the deeper water. (Tidal effects will be accounted for later). Since these three peak spectral frequencies represent wave periods of 19.6, 14.7, and 11.9 seconds, the frequency resolution is relatively poor. Thus, to improve frequency resolution, after the strongest peak was found for all frequency images, making use of the spectral overlap, a 3-point parabolic fit was made to the peak amplitude of this point and the corresponding points either side in frequency in the 3D spectral matrix. The peak amplitude of the fitted parabola was found, and its fitted peak frequency was determined from its location. Equation 1 was solved for the corresponding depth, D, iteratively, given the accurate peak location in the K_x-K_y plane. This was repeated for 88 of such images during the passage of the storm to estimate water depth for each of the 5 depths considered.

The local wave records are plotted in Figure 4 for the period either side of the storm passage, rising from near 2 meters after passage of an earlier storm, to near 4 meters at the storm peak, and falling to just less than a meter at the end. The RMS wave-height is plotted in the upper left plot of Figure 4, along with tide height time series, and the retrieved depths for the shallowest depth considered, 3.6 meters. The depths of the retrievals are labeled for each case. The black dots are the raw retrieved depths, while the red values represent depths corrected for tide height. The straight horizontal line represents the depth measured by the FRF. The depths estimated are seen to grow far above what they are expected to be near the peak RMS wave height achieved, based on this measure of propagation velocity of the waves onto shore.

Note that there is a lag in the error, relative to the peak wave height measured, that may be related to the fact that the swell continued to propagate onto shore, perhaps even growing in strength, as the RMS height receded. As we determined depth estimates by tracking the wave providing the strongest radar echo, typically the longest wave in the spectrum, the error in the method probably is related more to the swell amplitude and not the RMS wave amplitude, which was the only convenient wave height measure. This is in agreement with the fact that swell waves propagate according to a non-linear dispersion rule as they move into shallower water, becoming soliton like in behavior.

Figure 5 shows the summary of depth estimate errors for all depths considered plotted together. All errors approach the same value near 1-m RMS waveheight, but spread with higher wave height according with shallower true depth.

SUMMARY

We have analyzed 44 hours of marine radar data collected at the US Army Coastal Engineering Research Center Field Research Facility pier during the passage offshore of Hurricane Fran, in September of 1996. Each half hour, thirty two antenna rotations of data were collected covering 180^o of incident sea waves. The kinematics of the long waves were captured in a 3D Fourier Transform analysis of the imagery, for five different depths between 3.6 and 5.8 meters, as measured by the FRF staff. The expected locations of spectral energy for each of 8 wavenumber plots for 8 wave frequencies could be plotted using the linear ocean wave dispersion rule for shallow water. For RMS wave height less than 1 meter, the spectral peak typically fell where it should according to the linear dispersion rule for each depth considered. For higher waves, the spectral peak lay further off the expected position, and depths inferred by inverting the linear dispersion rule for gravity waves gave depth estimates that were in error.

Further work in this area is clearly warranted. A more thorough comparison with non-linear wave models is required, which is beyond the scope of the objectives stated here. The dependence on frequency resolution should be studied using longer time records than the 32 used here. However, this dependence is interleaved with the time period that a wave crest remains in the 32 x 32 pixel box used for analysis, and another set of wave crests entering it are not fully coherent with those exiting, so spectral broadening due to such effects is expected. Other methods discussed above for use in 3D Ω-K analysis are also beset by non-linear imaging mechanisms, so that there is no obvious choice as to a sensor for use in such analysis. Clearly, a sufficiently dense wave gauge array would serve such a purpose, but the difficulty in maintaining such in-situ sensors is well known. Thus, a remote sensing solution is clearly more viable from a cost-effectiveness and reliability perspective, particularly under the high sea conditions under which the non-linear effects become apparent. Thus, a measure of mean sea conditions, such as RMS wave height, collected at a single point in the area is necessary to apply non-linear models for reliable bathymetric retrieval.

These results suggest the need for a better non-linear model for the propagation of ocean waves in shallow water. Such a model has been proposed and is being tested (Shen, 2000). However, definition of a dispersion rule is not straightforward for such a non-linear model, and other inversion methods are under development (Chubb, et al, 2000).

ACKNOWLEDGEMENTS

We wish to thank the staff of the CERC FRF, headed by William Birkemeier, for providing the records of the wave fields used in this work, as well as the superb job of supporting us during the collection of the marine radar data. Todd Norrell was instrumental in analysis of all of the data, as well as helping developing analysis tools, during his tenure as a co-op engineering student at NRL.

REFERENCES

1. Young, I.R., W. Rosenthal, F. Ziemer, A three-dimensional analysis of marine radar images for the determination of ocean wave directionality and surface currents, JGR, **90**, C1, pp. 1049-1059, 1985.
2. Senet, C.M., J. Seemann, F. Ziemer, An iterative technique to determine the near surface current velocity from time series of sea surface images, Oceans '97, Halifax, 1997.
3. Dugan, J.P., H.H. Suzukawa, C.P. Forsythe, M.S. Farber, Ocean wave dispersions surface measured with airborne IR imaging system, IEEE Trans. Geosciences and Remote Sensing, **34**, pp. 1282-1284, 1996.
4. Dugan, J.P., C.P. Forsythe, H.H. Suzukawa, M.S. Farber, Bathymetry estimates from long range airborne imaging systems, Proc. 4th Int. Conf. On Remote Sensing for Marine and Coastal Environments, Orlando FL, 1997.
5. Stockdon, H.F., and R.A. Holman, Estimation of wave phase speed and nearshore bathymetry from video imagery, J. Geophysical Res., **105**, pp. 22,015-22,034, 2000.
6. Grilli, S.T., Depth inversion in shallow water based on nonlinear properties of shoaling periodic waves, Coastal Engineering, **35**, pp. 185-209, 1998.
7. Trizna, D.B., and D. Carlson, Studies of low grazing angle radar seascatter in nearshore regions, IEEE Trans. Geosciences and Remote Sensing, **34**, pp. 747-757, 1996.
8. Trizna, D.B., A model for Brewster angle damping and local multipath effects on low grazing angle sea scatter studies, , IEEE Trans. Geosciences and Remote Sensing, **35**, pp. 1232-1244, 1997.
9. Trizna, D.B., J. P. Hansen, P. Hwang, and J. Wu, Laboratory studies of radar sea spikes at low grazing angles, J. Geophys. Res., **96**, 12529-12537, 1991.
10. Trizna, D.B., Statistics of low grazing angle sea scatter for moderate and fully developed ocean waves, IEEE Trans. Antennas Propagation, **39**, 1361-1370, Dec., 1991.
11. C.Y. Shen, "Constituent Boussinesq Equations for Waves and Currents", submitted to J. Phys. Ocean..

12. Chubb, S. R., C. Y. Shen, D. B. Trizna, R. A. Fusina , Bathymetry Inversion Using Constituent Boussinesq Equations, IGARSS 2000, Honolulu, HI, 24-28 July 2000.

FIGURE CAPTIONS

Figure 1. An image of waves incident on shore, collected with a marine radar at the pier at Duck, NC, repeated each rotation 1.85-s apart for 32 images, every half hour. An echo from the pier end is seen about 25% in range downward, with a second laboratory-reflected and back to the pier echo seen at twice the distance, some 1,200 meters in range.

Figure 2. Eight wavenumber spectra for eight frequency cuts of 16 of the 3-D FFT image spectral output are shown for analysis of data similar to Fig.1. The red circle represents the expected peak position for the deep water dispersion rule, and white circle the shallow water for the FRF-measured depth shallow depth dispersion rule.

Figure 3. Similar to Figure 2, but for the highest wave conditions encountered. Note that the spectral peak locations are now off the expected radius defined by the shallow water dispersion rule.

Figure 4. Uncorrected (black) and tide-corrected (red) retrieved depths from the 3-D FFT analysis are plotted for the five depths, along with the RMS wave height (blue) and tide height (green). The error due to applying the linear model for increasing RMS wave height are plotted for each depth on the right.

Figure 5. Retrieved depth estimates for all five depths considered plotted together. The errors approach similar values for all depths at 1-m RMS wave height, and go to 0 for 0.8 m RMS wave height in all cases.

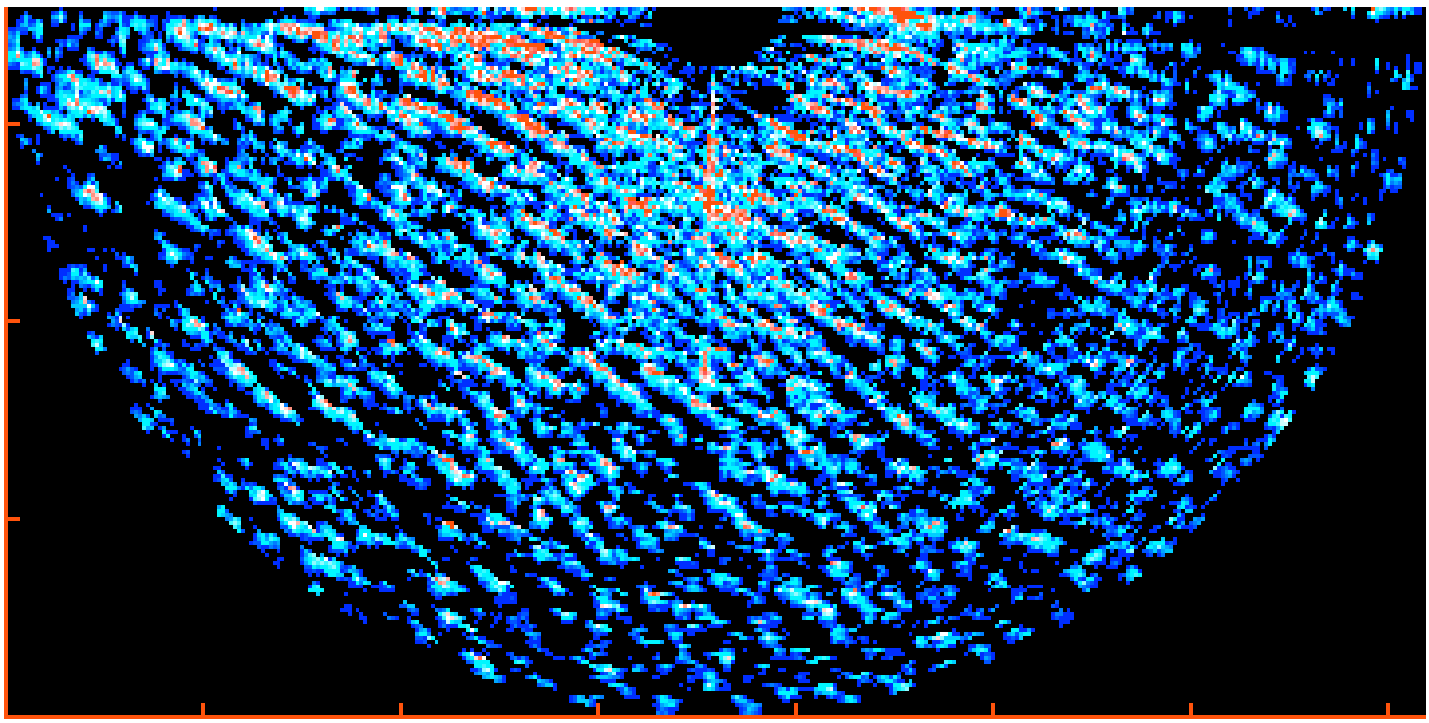

FIGURE 1

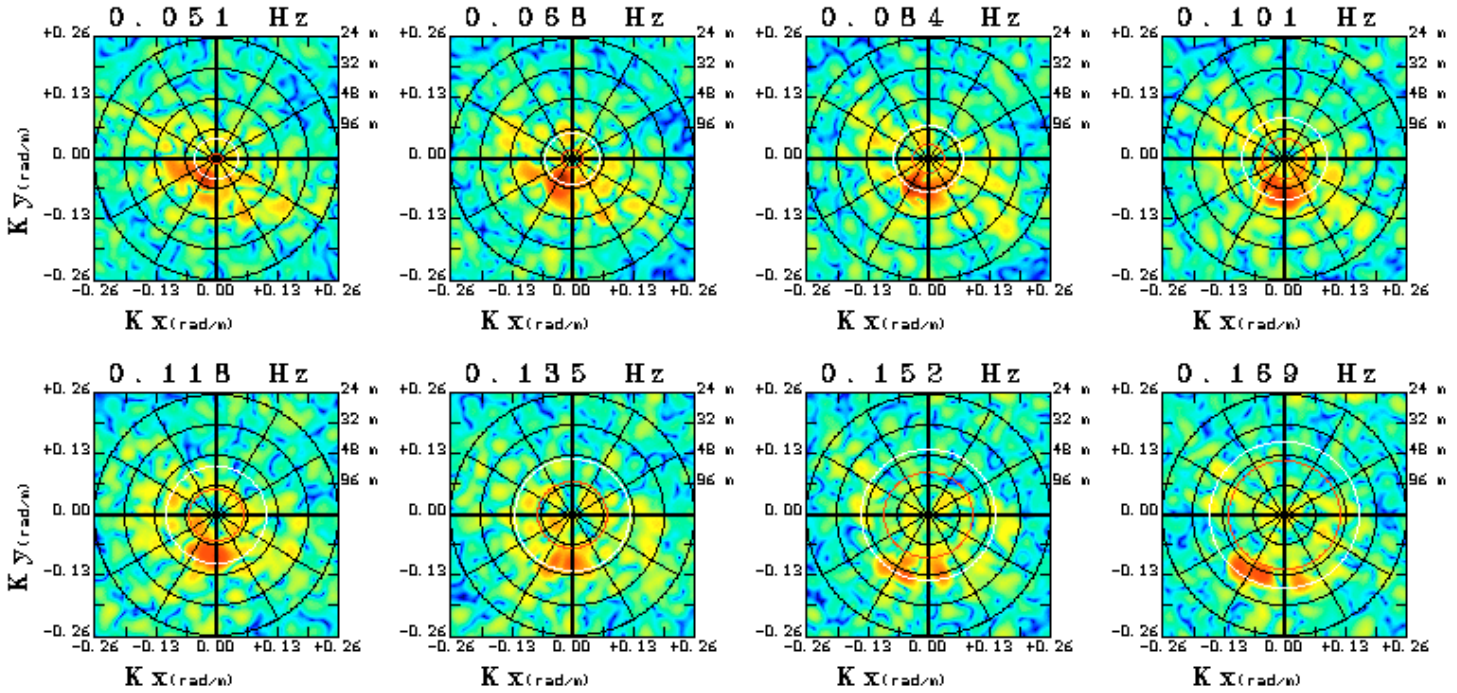
Duck 96, Julian Day 249 09:00
White circle depth = 5.8 m
0.051 Hz
0.068 Hz
0.084 Hz
0.101 Hz
0.118 Hz
0.135 Hz
0.152 Hz
0.169 Hz
24 m
32 m
48 m
96 m
+0.26
+0.13
0.00
-0.13
-0.26
Ky (rad/m)
Kx (rad/m)

FIGURES 2 & 3

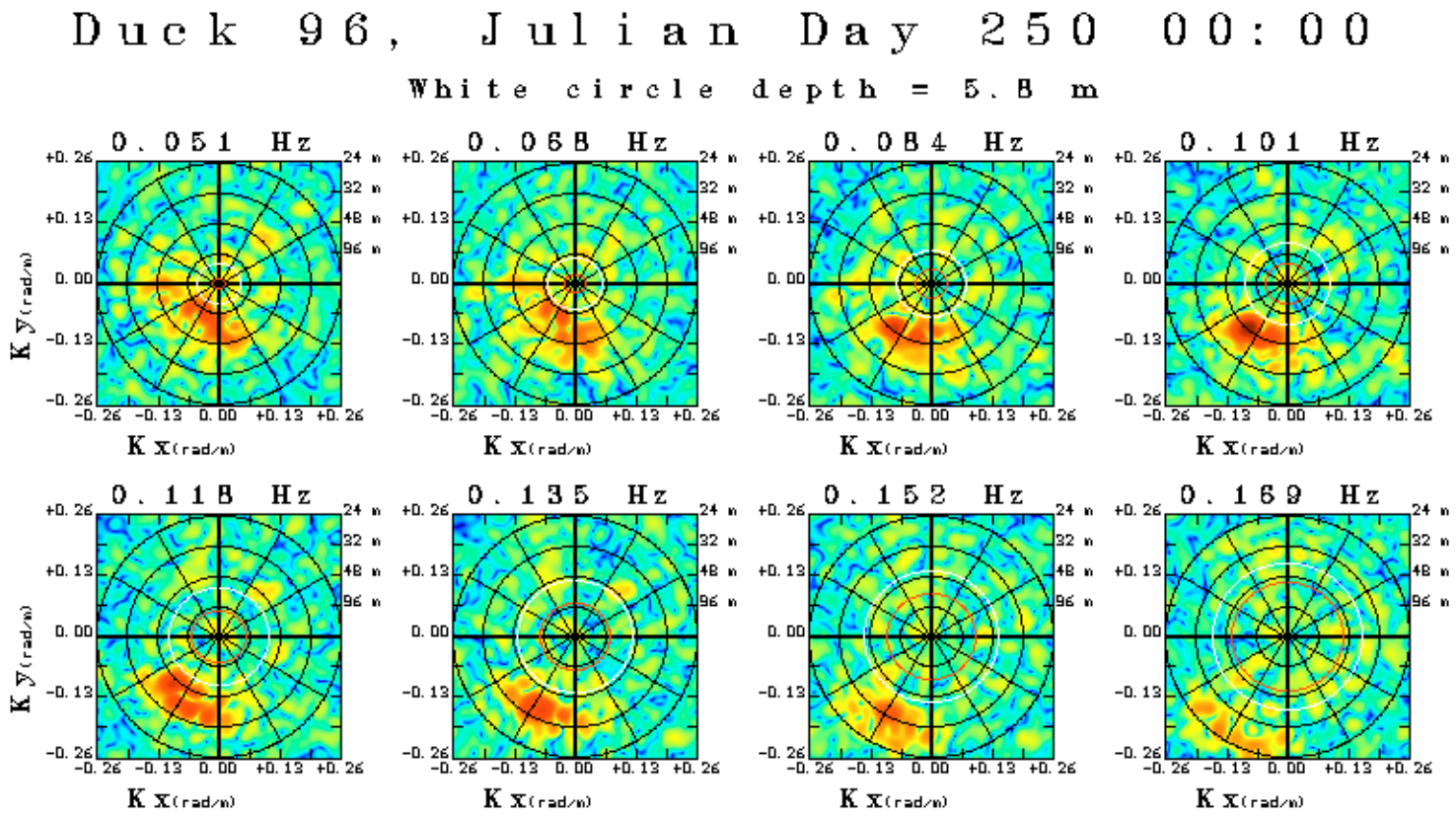
Duck 96, Julian Day 250 00:00
White circle depth = 5.8 m
0.051 Hz
0.068 Hz
0.084 Hz
0.101 Hz
0.118 Hz
0.135 Hz
0.152 Hz
0.169 Hz
24 m
32 m
48 m
96 m
+0.26
+0.13
0.00
-0.13
-0.26
Ky (rad/m)
Kx (rad/m)

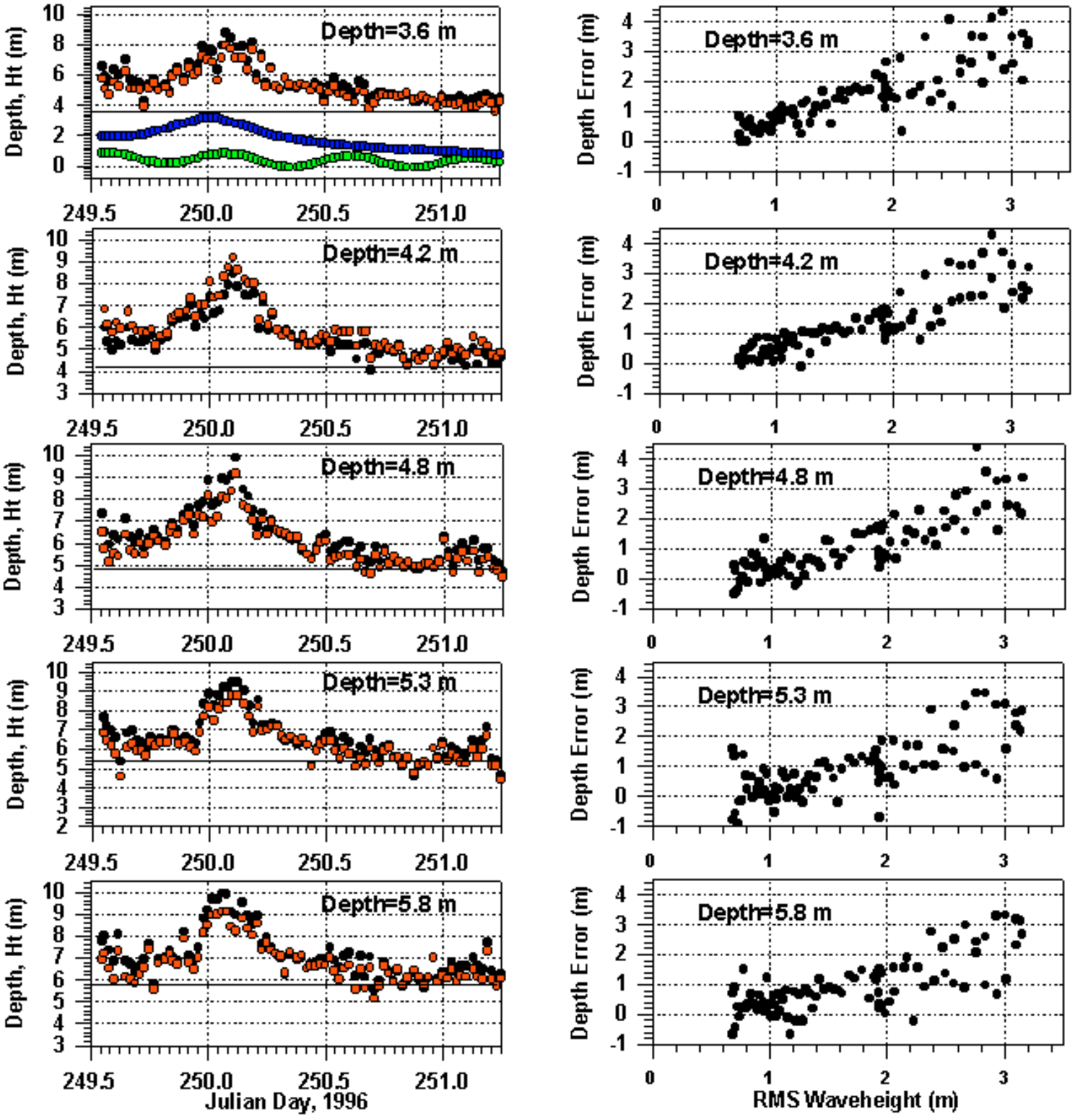
Depth=3.6 m
Depth=4.2 m
Depth=4.8 m
Depth=5.3 m
Depth=5.8 m
Depth, Ht (m)
Depth Error (m)
Julian Day, 1996
RMS Waveheight (m)
249.5
250.0
250.5
251.0
0
1
2
3

FIGURE 4

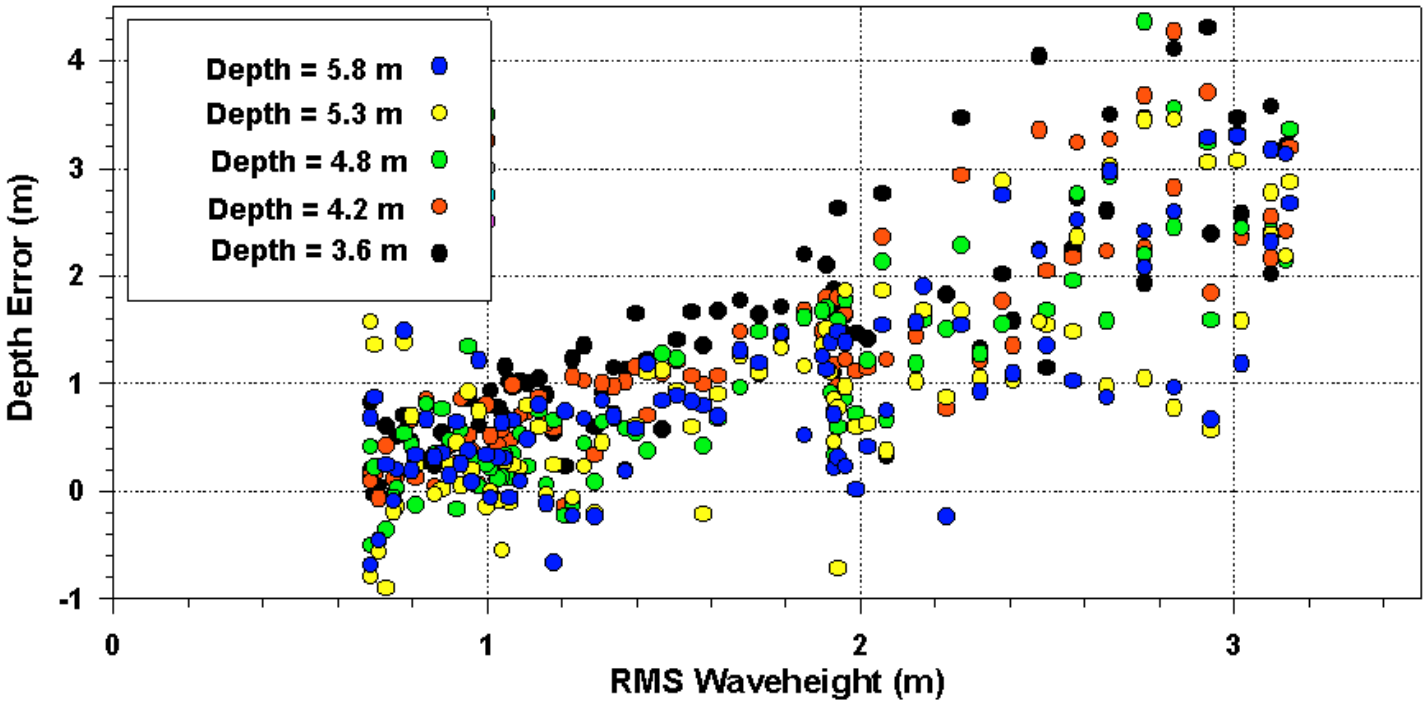
Depth = 5.8 m
Depth = 5.3 m
Depth = 4.8 m
Depth = 4.2 m
Depth = 3.6 m
Depth Error (m)
RMS Waveheight (m)
4
3
2
1
0
-1
0
1
2
3

FIGURE 5